Published in final edited form as:
Acta Biomater. 2013 January ; 9(1): 4889–4898. doi:10.1016/j.actbio.2012.08.029.

Bone regeneration in strong porous bioactive glass (13–93) scaffolds with an oriented microstructure implanted in rat calvarial defects

Xin Liu[1], **Mohamed N. Rahaman**[1,*], and **Qiang Fu**[2]

[1]Department of Materials Science and Engineering and Center for Bone and Tissue Repair and Regeneration, Missouri University of Science and Technology, Rolla, MO 65409, USA

[2]Materials Sciences Division, Lawrence Berkeley National Laboratory, Berkeley, CA 94720, USA

Abstract

There is a need for synthetic bone graft substitutes to repair large bone defects resulting from trauma, malignancy, and congenital diseases. Bioactive glass has attractive properties as a scaffold material but factors that influence its ability to regenerate bone in vivo are not well understood. In the present work, the ability of strong porous scaffolds of 13–93 bioactive glass with an oriented microstructure to regenerate bone was evaluated in vivo using a rat calvarial defect model. Scaffolds with an oriented microstructure of columnar pores (porosity = 50%; pore diameter = 50–150 μm) showed mostly osteoconductive bone regeneration, and new bone formation, normalized to the available pore area (volume) of the scaffolds, increased from 37% at 12 weeks to 55% at 24 weeks. Scaffolds of the same glass with a trabecular microstructure (porosity = 80%; pore width = 100–500 μm), used as the positive control, showed bone regeneration in the pores of 25% and 46% at 12 and 24 weeks, respectively. The brittle mechanical response of the as-fabricated scaffolds changed markedly to an elasto-plastic response in vivo at both implantation times. These results indicate that both groups of 13–93 bioactive glass scaffolds could potentially be used to repair large bone defects, but scaffolds with the oriented microstructure could also be considered for the repair of loaded bone.

Keywords

bone regeneration; bioactive glass scaffold; rat calvarial defect model; mineralization; mechanical response

1. Introduction

There is a clinical need for the development of synthetic scaffolds to repair large bone defects. In particular, the replacement of structural bone loss remains a challenging clinical problem. Millions of patients in the United States alone suffer each year from considerable bone loss resulting from trauma, malignancy, and congenital diseases, and this number is expected to increase substantially with the doubling of the population over the age of 65

*Corresponding author: Tel.: 1-573-341-4406; fax: 1-573-341-6934, rahaman@mst.edu (M. N. Rahaman).

years [1, 2]. Autogenous bone grafts, the gold standard for treatment, suffer from problems such as limited supply and donor site morbidity. Bone allografts are alternatives but they are expensive, and carry the risk of disease transmission and adverse host immune reaction. The delivery of growth factors, such as bone morphogenetic protein-2 (BMP-2), from a biodegradable carrier matrix, such as collagen, is used clinically for fracture and spinal repair. However, growth factors are expensive, and concerns have been expressed about possible links of high levels of growth factors to cancer and other complications [3, 4]. These problems have increased the need for synthetic bone graft substitutes.

Bioactive glasses are promising scaffold materials for bone regeneration because of their ability to convert to hydroxyapatite (HA), the main mineral constituent of bone, as well as their proven osteoconductivity and their ability to form a strong bond with bone and soft tissues [5, 6]. However, three-dimensional (3D) scaffolds of bioactive glasses prepared by many conventional methods often lack the requisite combination of porosity and mechanical properties for the repair of load-bearing bones. The compressive strengths reported for bioactive glass scaffolds prepared by many conventional methods are often lower than or comparable to the values reported for human trabecular bone (2–12 MPa) [7–9].

In our previous work, a method based on unidirectional freezing of suspensions [10] was used to form strong porous scaffolds of silicate 13–93 glass with an oriented microstructure of columnar pores which might have potential application in loaded bone repair [11, 12]. Scaffolds (porosity = 50%; pore diameter = 50–150 μm), created by unidirectional freezing of organic (camphene)-based suspensions showed an elastic modulus of 11 ± 3 GPa, in the range of values reported for human cortical bone (5–15 GPa), and a compressive strength of 47 ± 5 MPa, compared to a value of 100–150 MPa for human cortical bone. Bioactive glass (13–93) scaffolds with a similar oriented microstructure have been shown to support the proliferation and function of osteogenic MLO-A5 cells in vitro [13] and the infiltration of soft (fibrous) tissue in a rat subcutaneous model [14]. However, the ability of those oriented scaffolds to support bone regeneration in vivo was not evaluated.

It is known that bone regeneration in implants cannot be well predicted from their ability to support soft tissue infiltration, and that the microstructure and mechanical properties of porous scaffolds have a marked effect on host response [15]. Based on the promising mechanical properties and favorable microstructure of the “oriented” 13–93 bioactive glass scaffolds observed in our previous work, one objective of the present study was to evaluate the ability of the scaffolds to support bone regeneration and integration in an animal model. Another objective was to test the mechanical response of the scaffolds after implantation in vivo. Implants were evaluated using histomorphometry, electron microscopy, and mechanical testing techniques 12 and 24 weeks postimplantation. A rat calvarial defect model was used because it is a standard, inexpensive assay to study new bone formation in an osseous defect. Scaffolds of the same glass (13–93) with a microstructure similar to dry human trabecular bone were selected as the positive control group in order to study microstructural effects on bone regeneration; untreated defects served as the negative control group.

2. Materials and Methods

2.1 Preparation of bioactive glass (13–93) scaffolds

Scaffolds of 13–93 bioactive glass (composition 53SiO_2, 6Na_2O, 12K_2O, 5MgO, 20CaO, 4P_2O_5; wt %) with an oriented microstructure (referred to as “oriented” scaffolds) were prepared by unidirectional freezing of organic (camphene)-based suspensions using a method described in our previous work [11]. Scaffolds of the same bioactive glass with a microstructure similar to dry human trabecular bone (referred to as “trabecular” scaffolds),

the positive control group, were prepared using a polymer foam replication technique, as described in detail elsewhere [14]. The open porosity and pore size distribution of the scaffolds were measured using the Archimedes method and liquid extrusion porosimetry, respectively, as described previously [11, 16]. Table I summarizes the characteristics of the two groups of scaffolds. The as-fabricated constructs were sectioned and ground to form thin discs (4.6 mm in diameter × 1.5 mm), washed twice with deionized water and ethanol, dried, and dry-heat sterilized (12 h at 250 °C) prior to implantation.

2.2 Animals and surgical procedure

All animal experimental procedures were approved by the Animal Care and Use Committee, Missouri University of Science and Technology. Twenty-six male Sprague Dawley rats (3 months old; weight = 350–400 g) were maintained in the animal facility for 2 weeks to become acclimated to diet, water, and housing under a 12 hour/12 hour light/dark cycle. The rats were anesthetized with a combination of ketamine (72 mg/kg) and xylazine (6 mg/kg) and maintained under anesthesia with ether gas in oxygen. The surgical site was shaved and scrubbed with iodine. Using sterile instruments and aseptic technique, a 2 cm cranial skin incision was made in an anterior to posterior direction along the midline. The subcutaneous tissue, musculature and periosteum were dissected and reflected to expose the calvaria. A full-thickness defect (4.6 mm in diameter) was created in the central area of each parietal bone using a saline-cooled trephine drill to prevent overheating of the bone margins and to remove the bone debris. The dura mater was not disturbed. The bone defects were randomly implanted with disc-shaped bioactive glass scaffolds (4.6 mm in diameter × 1.5 mm) from each group (oriented or trabecular microstructure) or left empty. The periosteum and skin were repositioned and closed using wound clips. All animals were intramuscularly given a dose of ketoprofen (3 mg/kg), and allowed to recover. The condition of the surgical wound, food intake, activity, and clinical signs of infection were monitored daily. After 12 and 24 weeks, the animals were sacrificed by CO_2 inhalation, and the calvarial defect sites with surrounding bone and soft tissue were harvested for subsequent evaluation.

2.3 Synchrotron X-ray micro-computerized tomography analysis

Harvested samples from each group were analyzed using synchrotron X-ray micro-computerized tomography (SR microCT) at the Advanced Light Source synchrotron facility at the Lawrence Berkeley National Laboratory, Berkeley, CA. The samples were analyzed in a monochromatic X-ray beam of 22 keV and a resolution size of 1.7 μm voxels. The transmitted X-rays were imaged via a scintillator, magnifying lens, and digital camera. The samples were scanned in the absorption mode, and the images were obtained using a filtered back-projection algorithm. In this mode, the gray scale values of the reconstructed image are representative of the absorption coefficient.

2.4 Histology

The harvested samples were fixed in 10% buffered formaldehyde for 3 days, and then transferred into 70% ethyl alcohol. Each sample was carefully cut in half using a diamond wire saw (Model 850, South Bay Technology Inc., San Clement, CA) for paraffin-embedding and poly(methylmethacrylate) (PMMA)-embedding respectively. Tissue samples for paraffin sections were decalcified in 14 % ethylenediaminetetraacetic acid (EDTA) solution for 8 weeks, dehydrated in a series of graded ethanol, and embedded in paraffin. Longitudinal sections cut at 5 μm were used for hematoxylin and eosin (H&E) staining.

The undecalcified samples were embedded in PMMA. The fixed samples were dehydrated using ethanol, infiltrated with MMA monomer and polymerized [17]. The samples were affixed to acrylic slides and ground down to 40 μm using a surface grinder (EXAKT 400CS, Norderstedt, Germany). The plastic sections were stained using the von Kossa technique

[18]. Transmitted light images of the stained sections were taken with an Olympus BX 50 microscope connected with a CCD camera (DP70, Olympus, Japan).

2.5 Histomorphometric analysis

Light micrographs of H&E stained sections were used for histomorphometric analysis of bone regeneration within the defects. The entire defect area was measured, from one edge of the original calvarial bone, including the glass scaffold and tissue within, to the other edge of the host bone. Bone regeneration and the pore phase within this area were outlined and measured using NIH Image J software. Total bone regeneration was determined using 2 methods: (1) by normalizing the area of new bone to the total defect area, and (2) by normalizing the area of new bone to the available area of the pore phase in the scaffolds. Von Kossa positive area was determined from light micrographs of von Kossa stained sections. The dark area indicating mineralization was outlined and measured by NIH Image J, and the percent mineralization was normalized to the total defect area. For each implantation time, 5 samples for each group were evaluated, and the results are presented as a mean ± standard deviation.

2.6 Scanning electron microscopy and energy-dispersive X-ray analysis

Unstained sections of the implants in PMMA were coated with carbon and examined in a field-emission scanning electron microscope, FE-SEM (S-4700; Hitachi, Tokyo, Japan) equipped with an energy dispersive X-ray (EDS) spectrometer (Apollo X; EDAX, Inc.) to analyze morphological and compositional changes resulting from the bioactive glass conversion. The observations were performed at an accelerating voltage 15 kV and a working distance of 12 mm. The Ca/P atomic ratio was determined using the EDAX Genesis program, with synthetic hydroxyapatite and 13–93 glass as standards. Three randomly selected regions were analyzed, and the results are presented as a mean ± standard deviation.

2.7 Mechanical testing

After the animals were sacrificed, the bioactive glass implants with a layer of surrounding bone were removed using a trephine drill (inner diameter = 5 mm). The host bone surrounding the implants was trimmed with dental burs, leaving a disc-shape sample ~4.6 mm in diameter and ~ 1.5 mm in thickness. The implants were wrapped in gauze previously soaked in phosphate-buffered saline (PBS) to limit drying, kept at −20°C, and thawed to room temperature before testing [19]. The mechanical response of the implants was evaluated using a diametral compression test [20]. This test was used because of the small, disc-shaped geometry of the implants. The test is valid for determining the tensile strength of materials that show elastic deformation prior to failure. However, it has also been used to compare the response of materials that deform plastically [21–23] by considering the load to failure.

For each group, 5 samples were tested at each implantation time (deformation rate = 0.5 mm/min). After testing, the samples were freeze-dried (Freezezone 4.5, Labconco Corp., Kansas City, MO) to maintain the as-fractured morphology, mounted in epoxy resin, sectioned, and polished. The polished cross sections were coated with carbon and examined in an FE-SEM (Hitachi; S-4700) using the backscattered electron (BSE) mode at an accelerating voltage of 15 kV and a working distance of 13 mm.

For comparison, as-fabricated bioactive glass scaffolds with the oriented microstructure and dimensions similar to those of the implants (5 mm in diameter × 1.5 mm) were immersed in simulated body fluid (SBF) [24] at 37°C for 12 and 24 weeks, and tested under the same conditions. Five samples were tested for each immersion time.

2.8 Statistical analysis

The results are presented as a mean ± standard deviation. For each group of bioactive glass implants, analysis for differences in total bone regeneration and von Kossa positive area between implantation times was performed using one-way analysis of variance (ANOVA) with Tukey's post hoc test; differences were considered significant for $p < 0.05$.

3. Results

The microstructural and mechanical properties of the as-fabricated oriented and trabecular scaffolds used in the present study were similar to those described in our previous work [11, 16]. They are summarized in Table I, and images of the cross sections are shown in Fig. 1 for reference.

3.1 Bone regeneration and integration

SR microCT images of the scaffolds in the rat calvarial defects 12 and 24 weeks postimplantation (Fig. 2) allowed observation of bone regeneration and integration of the scaffolds with host bone. The images shown are for a plane half-way along the thickness of the implant. The differences in gray-scale in the images resulted from atomic mass and density differences of the elements in the material [25]. The unconverted bioactive glass, calcium phosphate material resulting from the glass conversion, and mineralized tissue have a higher calcium concentration and they showed a light-gray color. In comparison, soft tissue and calcium-depleted regions within the implants were dark-gray.

Twelve weeks postimplantation, new bone formation was found mainly within the oriented scaffold, with little new bone ingrowth and integration at the periphery (edge) of the implants (as revealed by the gaps at the interface between the implant and host bone) (Fig. 2a). Bone regeneration was higher at 24 weeks, and there was better integration between the scaffold and host bone (Fig. 2b). In comparison, the trabecular scaffolds showed new bone growth predominantly at the periphery of the scaffolds at 12 weeks, and there was good integration of the scaffold with host bone (Fig. 2c). At 24 weeks, bone regeneration was higher within the scaffolds and at the periphery (Fig. 2d).

Transmitted light images of H&E stained sections of the oriented and trabecular scaffolds implanted for 12 and 24 weeks in the rat calvarial defects are shown in Fig. 3. Twelve weeks postimplantation, new bone formation (B) and bridging of the defect occurred predominantly on the bottom (dural side) of the oriented implant (Fig. 3a, c). Bone regeneration in the implants and integration with host bone (O) was higher at 24 weeks (Fig. 3b, d). In comparison, the trabecular implants showed new bone growth (B) predominantly at the periphery of the implants, with little new bone formation on the dural side at 12 weeks (Fig. 3e). The amount of bone ingrowth was higher at 24 weeks, both at the periphery and on the dural side of the implants, and bony "islands" were present within the implants (Fig. 3f). In general, bone regeneration and integration observed from the H&E stained sections are compatible with the observations from the SR microCT images discussed previously. In the untreated defects, a thin layer of new bone was found at the defect margin after 12 weeks, and most of the defect was filled with compressed fibrous connective tissue. A thin layer of bone formed after 12 weeks failed to bridge the defect after 24 weeks (Fig. 3g, h).

Histomorphometric analysis showed that total bone regeneration in the implants increased significantly from 12 to 24 weeks (Fig. 4). For the oriented implants, total bone regeneration normalized to the total defect area was 18 ± 3% at 12 weeks and 24 ± 2% at 24 weeks. When normalized to the available pore area in the scaffolds, total bone regeneration was 37 ± 8% and 55 ± 5% at 12 and 24 weeks, respectively. Total bone regeneration in the trabecular implants was 19 ± 9% and 36 ± 12% at 12 and 24 weeks, respectively, when

normalized to the total defect area; when normalized to the area of the pore phase, the values were 25 ± 12% and 46 ± 13% at 12 and 24 weeks, respectively.

3.2 Mineralization of bioactive glass implants

Conversion of the oriented bioactive glass implants to an HA-like material in the rat calvarial defects was examined in an FE-SEM using BSE imaging for differences in phase and EDS mapping for elemental distributions of Ca (K), P (K), and Si (K) (Fig. 5). Twelve weeks postimplantation, BSE images of planar sections of the implants showed 3 regions: a light-gray inner core, a darker transition region, and a light-gray outer layer (Fig. 5a). Based on the EDS mapping (Figs. 5b–d), the inner core, rich in Ca and Si, was presumably an unconverted glass core (denoted G). The transition layer was found to be a Si-rich layer with low concentration of Ca and P (denoted S), while the outer layer, rich in Ca and P, was the converted layer, presumably an HA-like material (denoted H). At 24 weeks, the unconverted glass core had almost disappeared, leaving a Si-rich core (S), and the HA-like outer layer (H) was thicker.

The Ca/P atomic ratios in the different regions of the implants are shown in Table II. The Ca/P ratios in the regions of newly formed bone and the converted (HA-like) layer at 12 and 24 weeks were comparable to the value for stoichiometric HA (1.67). The glass region had a high Ca/P ratio (6.4 ± 0.4), comparable to the theoretical value for 13–93 glass (6.5). At 12 weeks, the Ca/P ratio of the Si-rich layer (2.6 ± 0.2) was between the values for HA and the glass. With an increase in the implantation time to 24 weeks, the Ca/P ratio of the Si-rich region decreased to 1.9 ± 0.1. For both implantation times, the tissue appeared to bond directly to the outer converted layer (H) of the implant. The presence of microcracks in the implant and the gap between the bone (B) and the surface of the implant (H) in Fig. 5a was presumably caused by capillary stresses during drying of the implant and by shrinkage stresses during embedding in PMMA.

Von Kossa stained images (Fig. 6) showed the mineralized phase in the defects. The positive stained areas indicated the presence of phosphate material [26]. Both the newly formed bone and the HA-like converted layer of the scaffold were stained dark whereas the unconverted glass (low in phosphate content) transmitted light. The regions of new bone formation were similar to those observed previously in the H&E stained sections. For both groups of implants, the total mineralized area, normalized to the total defect area, increased significantly with implantation time from 12 to 24 weeks (Fig. 7), as a result of the increase in bone regeneration and conversion of the bioactive glass implant to an HA-like material.

3.3 Mechanical response of bioactive glass implants

The response of the bioactive glass scaffolds (applied force vs. displacement) determined in the diametral compression test is shown in Fig. 8. The results are shown for the oriented scaffolds as fabricated and after immersion in SBF for 12 and 24 weeks, and for the oriented and trabecular scaffolds implanted in rat calvarial defects for 12 and 24 weeks. (The curves were arbitrarily shifted along the *x*-axis to maintain clarity.) As fabricated, the oriented scaffolds showed a typical elastic response followed by failure: the load increased almost linearly with deformation before fracture at a load of 88 ± 17 N. After immersion in SBF, an elastic response was still observed but the load at fracture decreased markedly, to 38 ± 5 N at 12 weeks and 34 ± 7 N at 24 weeks. As shown for trabecular scaffolds of 13–93 glass, the decrease in compressive strength as a function of immersion time in SBF can be modeled in terms of a reduction in the effective cross sectional area of the glass struts for load bearing due to conversion of the surface layer of the glass to a mesoporous HA-like material [27]. However, additional factors, such as an increase in the critical flaw size resulting from corrosion in SBF, could also contribute to the decrease in failure load.

In comparison, the scaffolds showed a markedly different mechanical response after implantation in vivo. An elasto-plastic response was observed, in which the load initially increased approximately linearly with deformation (Region 1), followed by Region 2 in which the deformation showed a large increase with a small change in load, and finally Region 3 in which the load increased more steeply, presumably due to compaction of the sample. For the oriented implants, the load at the yield point (taken as the load at approximately the elastic limit) was ~11 N at 12 weeks, and it showed little increase (to ~13 N) at 24 weeks. The trabecular scaffolds implanted for 12 weeks were too weak to be tested in the mechanical testing machine; 24 weeks postimplantation, the load at the yield point was ~4 N.

The load vs. displacement response of the scaffolds after implantation in vivo showed a large degree of scatter which is believed to result from two main sources. First, the size of the implants used in the rat calvarial defect model was small (4.6 mm × 1.5 mm); as a result, small variations in the overall geometry can have a marked effect on the mechanical response. Second, the distribution of new bone within the implants was not homogeneous; for the implantation times used, new bone infiltrated only the lower part of the oriented scaffolds.

The energy absorbed during the deformation of the scaffolds was estimated from the area under the force vs. displacement curve [28]. For the scaffolds implanted in vivo, the area was determined up to a deformation of 40%, which corresponded approximately to the deformation at which compaction of the sample started to occur. For the oriented scaffolds implanted for 12 and 24 weeks, the energy absorbed during the deformation (20 mJ) was 2–3 times the value of the as-fabricated scaffolds and ~20 times the values for the oriented scaffolds immersed in SBF for similar periods.

4. Discussion

The results of the present work provided new information for the potential use of strong porous bioactive glass (13–93) scaffolds with an oriented microstructure in bone repair. In particular, the results provided information on the ability of the oriented implants to regenerate bone and integrate with host bone, and on the mineralization and mechanical response of the implants in a bone defect model. While the animal model used was a non-loaded bone defect model, the results are useful for designing scaffolds to be used in the more demanding application of loaded bone regeneration.

4.1 Bone regeneration and integration

While the oriented and trabecular scaffolds were both capable of supporting bone regeneration in rat calvarial defects, the microstructure strongly influenced the way in which new bone infiltrated the implant and the integration of the implant with host bone (Figs. 2, 3). Twelve weeks postimplantation, new bone formed mainly on the dural (bottom) side of the oriented implants, with little bone ingrowth into the periphery (edge) of the implants. At 24 weeks, there was an improvement in total bone regeneration, bone infiltration into the periphery of the implants, and integration with host bone were higher. In comparison, the trabecular implants showed bone regeneration predominantly into the periphery of the implants and better integration with host bone than the oriented implants at 12 weeks (Figs. 2, 3).

The difference in bone infiltration in the two groups of scaffolds (at the periphery versus the dural side) may result from differences in the scaffold architecture. Previous studies have shown that in addition to porosity and pore size, other factors such as pore interconnectivity, the size of the opening between adjacent pores, permeability, and microstructural anisotropy

of the scaffolds can have an important effect on bone infiltration [29–30]. Whereas the trabecular scaffolds had a larger porosity (~80%) and pore size (100–500 μm), the more tortuous pore channels could limit bone ingrowth to the periphery. In comparison, the oriented scaffolds had a lower porosity (~50%), and the pore diameter (50–150 μm) was comparable to the minimum pore size shown to be favorable for bone ingrowth [31, 32]. However, the oriented pores were connected at several positions along their length, and the pore channels were less tortuous, which could facilitate bone ingrowth into the interior of the scaffolds. Despite the larger pore size, new bone formation in the trabecular scaffolds based on the available pore area (volume) was 46 ± 13%, compared to 55 ± 5% for the oriented scaffolds (Fig. 4b). This might be a further indication that the tortuosity of the pore channels played an important role in controlling bone infiltration in the scaffolds.

It has been observed that the dura mater, pericranium, and surrounding bone can each influence osteogenesis differently in rabbit calvarial defects [33]. The dura was more osteogenic than the pericardium, and it appeared to be the source of bone growth on the dural side and in the interior of implants, whereas the pericranium appeared to enhance bone growth into the periphery. Since the mechanism of bone growth at the periphery could be different from that into the interior of the scaffolds, the architecture of the scaffolds could also influence bone growth at the periphery relative to the interior. Apparently, the trabecular microstructure was more conducive to bone growth from the pericranium and surrounding bone, whereas the oriented microstructure was better at supporting bone ingrowth from the dura mater.

In practice, the method used to create the oriented scaffolds used in this study (unidirectional freezing of suspensions) has a limited ability for substantially increasing the pore diameter of the scaffolds. Furthermore, an increase in the pore diameter is achieved mainly at the expense of lowering the mechanical properties of the scaffolds [11]. Consequently, use of these oriented bioactive glass implants for the repair of loaded bone may require additional considerations for accelerating bone ingrowth and integration.

4.2 Mineralization of scaffolds in vivo

A distinctive property of bioactive glasses is their conversion to an HA-like material (mineralization) in vivo [5, 6]. The HA-like layer grows as conversion of the bioactive glass continues with time, leading to a continuous degradation of the scaffold mechanical properties. Conversion of a bioactive glass in vitro (in SBF) is sometimes used as a guide to its mineralization in vivo, but the in vitro kinetic data might not be very applicable to the in vivo environment. The results of this study showed that 13–93 glass converted faster in rat calvarial defects than in SBF in vitro. SEM showed that after immersion in SBF for 24 weeks, the oriented scaffolds consisted of a converted layer ~10 μm thick, an SiO_2-rich layer (~3 μm), and a considerable amount of unconverted glass (results not shown). In comparison, 24 weeks postimplantation, the oriented scaffolds were almost completely converted to an HA-like material (~30 μm thick) surrounding a SiO_2-rich core, with little unconverted glass (Fig. 5). The faster conversion of 13–93 bioactive glass in vivo presumably resulted from the more dynamic environment of the body (compared to the more static in vitro system), and the presence of electrolytes, proteins, and biological polymers in the body fluid [34, 35].

An interesting observation was that EDS analysis showed the presence of Si in the converted layer of the bioactive glass, with a concentration gradient from the SiO_2-rich interior to the surface of the implant (Fig. 5). Apart from a difference in rate, the conversion of 13–93 bioactive glass to HA appears to follow a mechanism similar to that of 45S5 bioactive glass [5], resulting in the formation of an HA-like material surrounding an SiO_2-rich core. Previous studies have suggested that degradation of the SiO_2-rich core occurred

continuously by cellular resorption and Si transport through the HA-like material, followed by Si dissolution [35, 36]. The solubility of silica in water is ~0.015 wt% at 37 °C [37], and silicon substitution in HA is <2 wt% [38]. The observed Si concentration in the implants may be due to degradation of the SiO_2-rich core and transport from the high concentration at the interface with the HA-like material to the low concentration at the surface of the implant.

4.3 Mechanical response of scaffolds in vitro and in vivo

Another interesting finding of the present study was the marked difference in mechanical response between the scaffolds after immersion in SBF in vitro (elastic response in which the load to failure decreased with immersion time) and after implantation in vivo for 12 and 24 weeks (elasto-plastic response) (Fig. 8). This difference presumably resulted mainly from the infiltration of new bone and soft tissue into the scaffolds in vivo. A composite structure was formed, consisting of unconverted glass, HA-like material formed by partial conversion of the glass, and tissue (new bone and soft tissue) infiltrated into the pores of the scaffold (Fig. 5a, e). The infiltrated tissue presumably provided a deformable matrix for the brittle glass and HA-like material. Scaffolds implanted for 12 and 24 weeks in rat calvarial defects returned to their original geometry following the diametral compression test. SEM examination of the implants after testing (Fig. 9) showed that while the glass phase had fractured into several pieces, it was held together by the matrix composed of new bone and soft tissue.

The mechanical response of the bioactive glass scaffolds observed in this study is compatible with the results of recent studies which showed that the brittle failure of porous ceramics can be altered after implantation in vivo or after infiltration with polymers in vitro. Porous HA scaffolds, with a brittle response as fabricated, showed an elasto-plastic response in compression after implantation for 8 weeks in an rhBMP-2 driven ectopic bone model in muscle [39]. Coating or infiltrating porous glass or ceramic scaffolds with a biodegradable polymer resulted in an improvement in toughness and an elasto-plastic response in compression [40–42]. The toughness of the scaffolds, determined from the energy absorbed per unit volume during deformation, could be increased by 2–20 times after incorporation of the polymer phase [7, 40, 43]. Scaffolds with compressive strengths of ~0.1–0.5 MPa as fabricated, had toughness values of ~40–250 $kJ \cdot m^{-3}$ after coating or infiltrating with a polymer phase [43–45], while scaffolds with higher compressive strengths (~10 MPa) had toughness values up to ~1000 $kJ \cdot m^{-3}$ [41]. In the present study, the energy absorbed during deformation of the oriented scaffolds (implantation time = 12 or 24 weeks) was ~800 $kJ \cdot m^{-3}$, in the higher range of values reported for bioactive glass scaffolds coated or infiltrated with a polymer phase.

The results of the present in vivo study showed the ability of oriented bioactive glass (13–93) scaffolds to support bone regeneration, almost complete conversion within 24 weeks, and development of a desirable elasto-plastic response. In general, upon implantation of a bioactive glass scaffold in a bone defect, the strength of the scaffold decreases with time due to conversion of the glass to an HA-like material, but this should be countered by an increase in strength due to bone ingrowth. A key issue for application of these oriented scaffolds in loaded bone repair is matching the conversion rate of the glass with the rate of bone regeneration to provide the requisite mechanical properties. This issue is being addressed in our current work.

5. Conclusion

Strong porous scaffolds of 13–93 bioactive glass with an oriented microstructure of columnar pores (porosity = 50%; pores diameter = 50–150 μm) showed the capacity to regenerate bone in rat calvarial defects. Bone regeneration in the oriented implants

normalized to the available pore area (volume) increased from 37% at 12 weeks to 55% at 24 weeks. Scaffolds with a trabecular microstructure (porosity = 80%; pore width = 100–500 μm), used as the positive control, showed bone regeneration in the pores of 25% and 46% at 12 and 24 weeks, respectively. Conversion of the bioactive glass implants in vivo was more than 3 times faster than in vitro (immersion in simulated body fluid), resulting in almost complete conversion of the glass 24 weeks postimplantation. The mechanical response of the implants changed markedly from a brittle response in vitro (as fabricated or after immersion in simulated body fluid) to an elasto-plastic response after implantation in vivo for 12 or 24 weeks. Together, the results indicate promising potential for the use of these oriented bioactive glass scaffolds in the repair of loaded or non-loaded bone.

Acknowledgments

This work was supported by the National Institutes of Health, National Institute of Arthritis, Musculoskeletal and Skin Diseases (NIAMS), Grant # 1R15AR056119-01, and by the U.S. Army Medical Research Acquisition Activity, under Contract No. W81XWH-08-1-0765. The authors would like to thank Mo-Sci Corp., Rolla, MO for the bioactive glass used in this work, Dr. R. F. Brown for assistance with animal surgeries, and the Advanced Light Source, Lawrence Berkeley National Lab, for use of the dedicated X-ray tomography beamline.

References

1. U.S. Census Bureau. Interim State Population Projections. 2005.
2. U.S. Census Bureau. Health and nutrition. Washington, DC: U.S. Census Bureau statistical abstracts of the United States; 2009. p. 117
3. Thawani JP, Wang AC, Than KD, Lin CY, La Marca F, Park P. Bone morphogenetic proteins and cancer: review of the literature. Neurosurgery. 2010; 66:233–246. [PubMed: 20042986]
4. Pasche B. Role of transforming growth factor beta in cancer. J Cell Physiol. 2001; 186:153–168. [PubMed: 11169452]
5. Hench LL. Bioceramics. J Am Ceram Soc. 1998; 81:1705–1728.
6. Rahaman MN, Day DE, Bal BS, Fu Q, Jung SB, Bonewald LF. Bioactive glass in tissue engineering. Acta Biomater. 2011; 7:2355–2373. [PubMed: 21421084]
7. Fu Q, Saiz E, Rahaman MN, Tomsia AP. Bioactive glass scaffolds for bone tissue engineering: state of the art and future perspectives. Mater Sci Eng C. 2011; 31:1245–1256.
8. Baino F, Vitale-Brovarone C. Three-dimensional glass-derived scaffolds for bone tissue engineering: current trends and forecasts for the future. J Biomed Mater Res A. 2011; 97:514–535. [PubMed: 21465645]
9. Gerhardt L-C, Boccaccini AR. Bioactive glass and glass-ceramic scaffolds for bone tissue engineering. Materials. 2010; 3:3867–3910.
10. Deville S, Saiz E, Nalla RK, Tomsia AP. Freezing as a path to build complex composites. Science. 2006; 311:515–518. [PubMed: 16439659]
11. Liu X, Rahaman MN, Fu Q, Tomsia AP. Porous and strong bioactive glass (13-93) scaffolds prepared by unidirectional freezing of camphene-based suspensions. Acta Biomater. 2012; 8:415–423. [PubMed: 21855661]
12. Liu X, Rahaman MN, Fu Q. Oriented bioactive glass (13-93) scaffolds with controllable pore size by unidirectional freezing of camphene-based suspensions: microstructure and mechanical response. Acta Biomater. 2011; 7:406–416. [PubMed: 20807594]
13. Fu Q, Rahaman MN, Bal BS, Brown RF. Preparation and in vitro evaluation of bioactive glass (13-93) scaffolds with oriented microstructures for repair and regeneration of load-bearing bones. J Biomed Mater Res A. 2010; 93:1380–1390. [PubMed: 19911380]
14. Fu Q, Rahaman MN, Bal BS, Kuroki K, Brown RF. In vivo evaluation of 13-93 bioactive glass scaffolds with trabecular and oriented microstructures in a subcutaneous rat implantation model. J Biomed Mater Res A. 2010; 95:235–244. [PubMed: 20574983]
15. Place ES, Evans ND, Stevens MM. Complexity in biomaterials for tissue engineering. Nat Mater. 2009; 8:457–470. [PubMed: 19458646]

16. Fu Q, Rahaman MN, Sonny Bal B, Brown RF, Day DE. Mechanical and in vitro performance of 13-93 bioactive glass scaffolds prepared by a polymer foam replication technique. Acta Biomater. 2008; 4:1854–1864. [PubMed: 18519173]
17. Sanderson C, Kitabayashi LR. Parallel experience of two different laboratories with the initiator Perkadox 16 for polymerization of methylmethacrylates. J Histotechnology. 1994; 17:343–348.
18. Sheehan, D.; Hrapchak, B. Theory and Practice of Histotechnology. 2nd ed. St. Louis: CV Mosby Co.; 1980.
19. An, YH.; Draughn, RA. Mechanical Testing of Bone and the Bone-Implant Interface. Boca Raton, FL: CRC Press; 1999.
20. Thomas MB, Doremus RH, Jarcho M, Salsbury RL. Dense hydroxylapatite: fatigue and fracture strength after various treatments, from diametral tests. J Mater Sci. 1980; 15:891–894.
21. Xie D, Brantley WA, Culbertson BM, Wang G. Mechanical properties and microstructures of glass-ionomer cements. Dent Mater. 2000; 16:129–138. [PubMed: 11203534]
22. Womack WJ, Santoni BG, Puttlitz CM. Diametral compression of non-circular diaphyseal bone sections. J Biomech. 2008; 41:194–199. [PubMed: 17706657]
23. Sinka IC, Cunningham JC, Zavaliangos A. Analysis of tablet compaction. II. Finite element analysis of density distributions in convex tablets. J Pharm Sci. 2004; 93:2040–2053. [PubMed: 15236453]
24. Kokubo T, Kushitani H, Sakka S, Kitsugi T, Yamamuro T. Solutions able to reproduce in vivo surface-structure changes in bioactive glass-ceramic A-W. J Biomed Mater Res. 1990; 24:721–734. [PubMed: 2361964]
25. Fu Q, Huang W, Jia W, Rahaman MN, Liu X, Tomsia AP. Three-dimensional visualization of bioactive glass-bone integration in a rabbit tibia model using synchrotron X-ray microcomputed tomography. Tissue Eng Part A. 2011; 17:3077–3084. [PubMed: 21875330]
26. Bonewald LF, Harris SE, Rosser J, Dallas MR, Dallas SL, Camacho NP, et al. Von Kossa staining alone is not sufficient to confirm that mineralization in vitro represents bone formation. Calcified Tissue Int. 2003; 72:537–547.
27. Fu Q, Rahaman MN, Fu H, Liu X. Silicate, borosilicate, and borate bioactive glass scaffolds with controllable degradation rate for bone tissue engineering applications. I. Preparation and in vitro degradation. J Biomed Mater Res A. 2010; 95:164–171. [PubMed: 20544804]
28. Gibson, LJ.; Ashby, MF. Cellular Solids: Structure and Properties. 2nd ed.. Cambridge: Cambridge University Press; 1997.
29. Jones AC, Arns CH, Hutmacher DW, Milthorpe BK, Sheppard AP, Knackstedt MA. The correlation of pore morphology, interconnectivity and physical properties of 3D ceramic scaffolds with bone ingrowth. Biomaterials. 2009; 30:1440–1451. [PubMed: 19091398]
30. Otsuki B, Takemoto M, Fujibayashi S, Neo M, Kokubo T, Nakamura T. Pore throat size and connectivity determine bone and tissue ingrowth into porous implants: three-dimensional micro-CT based structural analyses of porous bioactive titanium implants. Biomaterials. 2006; 27:5892–5900. [PubMed: 16945409]
31. Hulbert SF, Young FA, Matthews RS, Klawitter JJ, Talbert CD. Potential of ceramic materials as permanently implantable skeletal prostheses. J Biomed Mater Res. 1970; 4:433–456. [PubMed: 5469185]
32. Karageorgiou V, Kaplan D. Porosity of 3D biomaterial scaffolds and osteogenesis. Biomaterials. 2005; 26:5474–5491. [PubMed: 15860204]
33. Gosain AK, Santoro TD, Song LS, Capel CC, Sudhakar PV, Matloub HS. Osteogenesis in calvarial defects: contribution of the dura, the pericranium, and the surrounding bone in adult versus infant animals. Plast Reconst Surg. 2003; 112:515–527. [PubMed: 12900610]
34. Fu Q, Rahaman MN, Day DE. Accelerated conversion of silicate bioactive glass (13-93) to hydroxyapatite in aqueous phosphate solution containing polyanions. J Am Ceram Soc. 2009; 92:2870–2876.
35. Radin S, Ducheyne P, Falaize S, Hammond A. In vitro transformation of bioactive glass granules into Ca-P shells. J Biomed Mater Res. 2000; 49:264–272. [PubMed: 10571915]

36. Schepers EJ, Ducheyne P. Bioactive glass particles of narrow size range for the treatment of oral bone defects: a 1-24 month experiment with several materials and particle sizes and size ranges. J Oral Rehabil. 1997; 24:171–181. [PubMed: 9131472]
37. Alexander GB, Heston WM, Iler RK. The solubility of amorphous silica in water. The J Phys Chem. 1954; 58:453–455.
38. Kim SR, Lee JH, Kim YT, Riu DH, Jung SJ, Lee YJ, et al. Synthesis of Si, Mg substituted hydroxyapatites and their sintering behaviors. Biomaterials. 2003; 24:1389–1398. [PubMed: 12527280]
39. Woodard JR, Hilldore AJ, Lan SK, Park CJ, Morgan AW, Eurell JA, et al. The mechanical properties and osteoconductivity of hydroxyapatite bone scaffolds with multi-scale porosity. Biomaterials. 2007; 28:45–54. [PubMed: 16963118]
40. Chen QZ, Boccaccini AR. Poly(D,L-lactic acid) coated 45S5 Bioglass®-based scaffolds: processing and characterization. J Biomed Mater Res A. 2006; 77:445–457. [PubMed: 16444684]
41. Peroglio M, Gremillard L, Gauthier C, Chazeau L, Verrier S, Alini M, et al. Mechanical properties and cytocompatibility of poly(ε-caprolactone)-infiltrated biphasic calcium phosphate scaffolds with bimodal pore distribution. Acta Biomater. 2010; 6:4369–4379. [PubMed: 20553981]
42. Martinez-Vazquez FJ, Perera FH, Miranda P, Pajares A, Guiberteau F. Improving the compressive strength of bioceramic robocast scaffolds by polymer infiltration. Acta Biomater. 2010; 6:4361–4368. [PubMed: 20566307]
43. Bretcanu O, Misra S, Roy I, Renghini C, Fiori F, Boccaccini AR, et al. In vitro biocompatibility of 45S5 Bioglass®-derived glass–ceramic scaffolds coated with poly(3-hydroxybutyrate). J Tissue Eng Regen M. 2009; 3:139–148. [PubMed: 19170250]
44. Kim HW, Knowles JC, Kim HE. Hydroxyapatite porous scaffold engineered with biological polymer hybrid coating for antibiotic vancomycin release. J Mater Sci Mater Med. 2005; 16:189–195. [PubMed: 15744609]
45. Baino F, Verne E, Vitale-Brovarone C. Feasibility, tailoring and properties of polyurethane/bioactive glass composite scaffolds for tissue engineering. J Mater Sci Mater Med. 2009

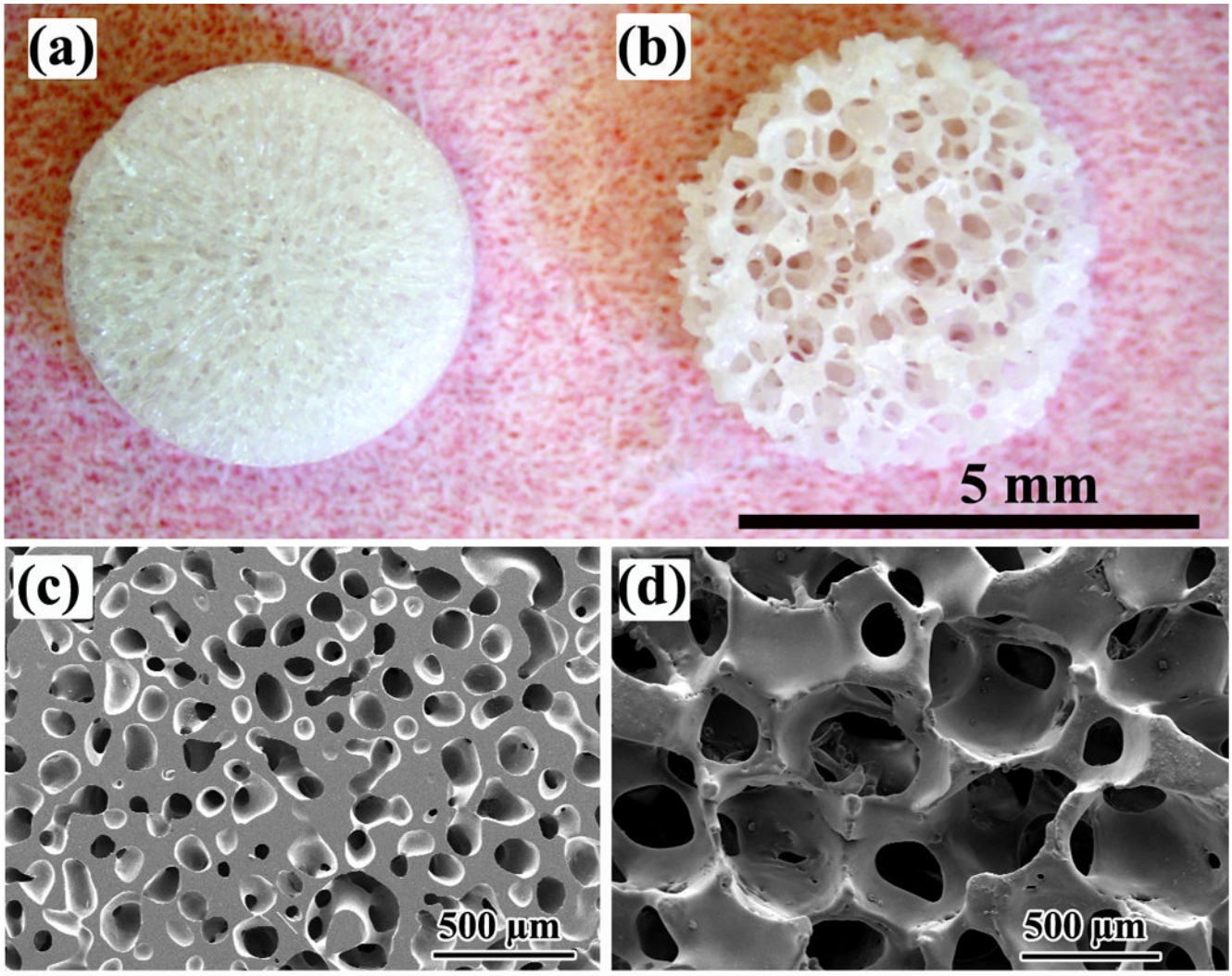

Fig. 1.

Optical images of disc-shaped bioactive glass (13–93) scaffolds with (a) an oriented microstructure and (b) a trabecular microstructure (positive control). SEM images of cross sections of the oriented and trabecular scaffolds are shown in (c) and (d), respectively. The cross section in (c) is perpendicular to the pore orientation direction.

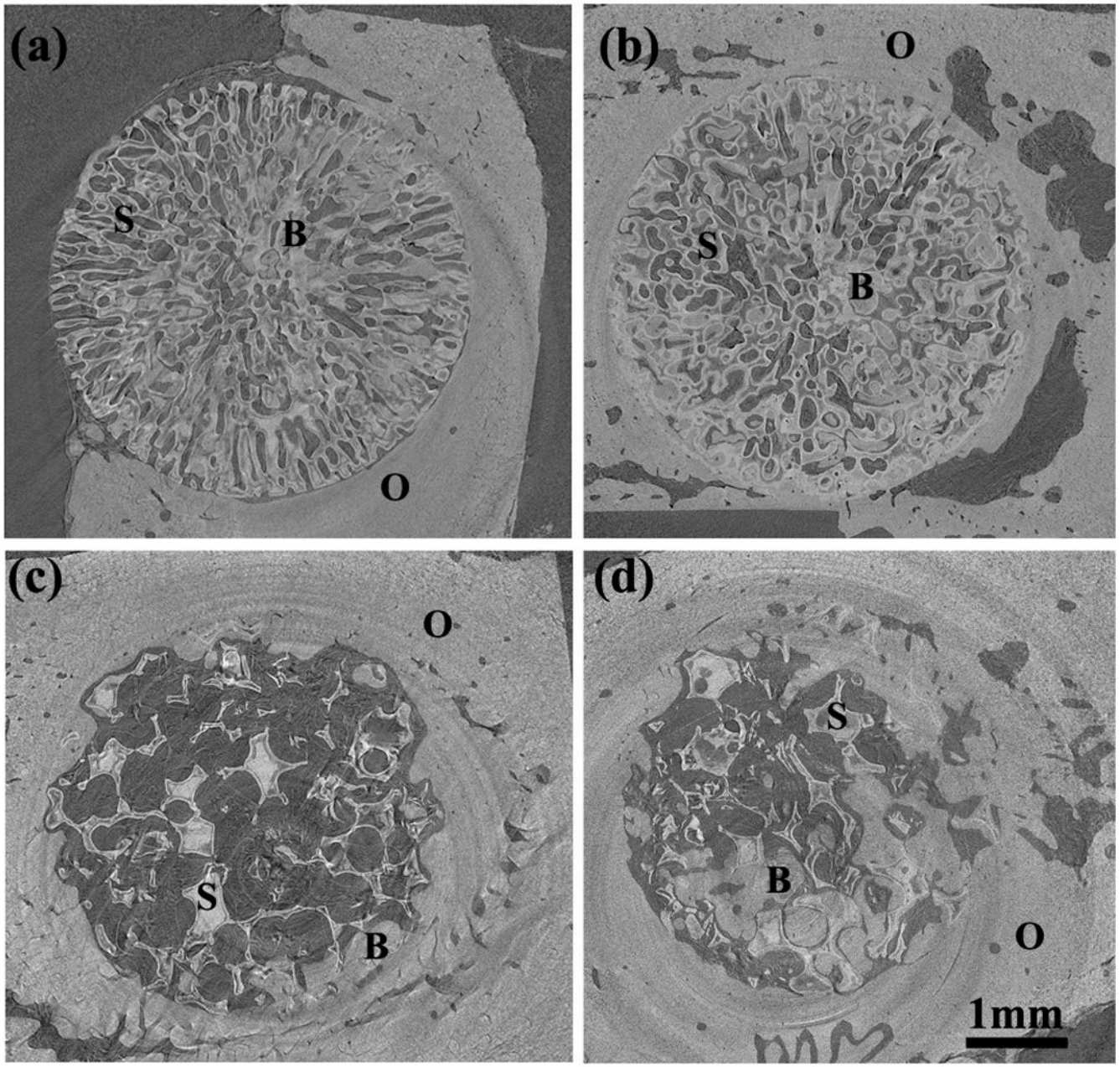

Fig. 2.

Synchrotron micro-computerized X-ray tomography (SR microCT) images of oriented scaffold after implantation for 12 weeks (a) and 24 weeks (b), and trabecular scaffold after implantation for 12 weeks (c) and 24 weeks (d). The distribution of old bone (O), new bone formation (B) and the bioactive glass scaffold (S) is shown.

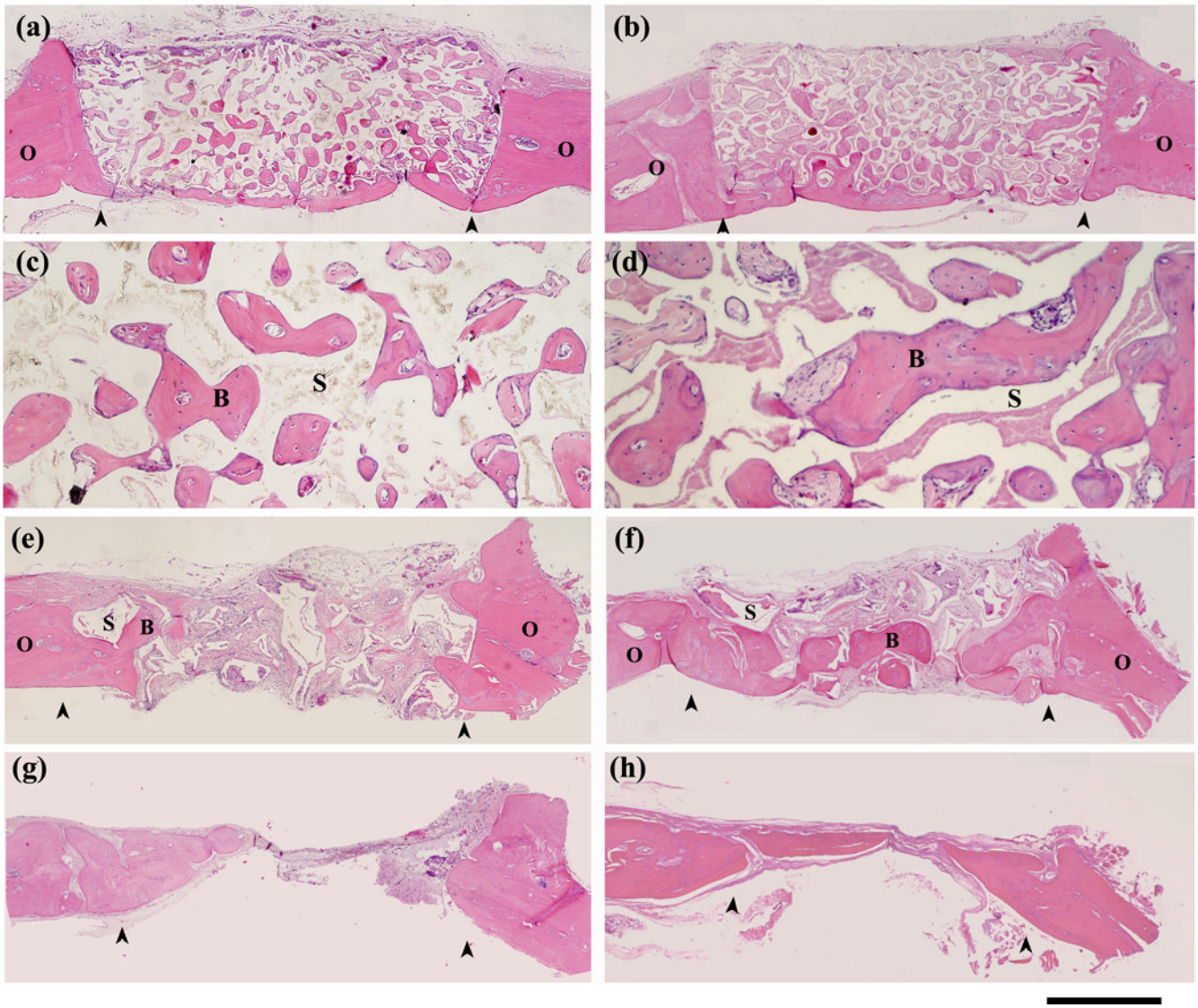

Fig. 3.

H&E stained sections of rat calvarial defects implanted with oriented scaffolds at 12 weeks (a, c) and 24 weeks (b, d); defects implanted with trabecular scaffolds at 12 weeks (e) and 24 weeks (f), and untreated defects at 12 weeks (g) and 24 weeks (h). Stained sections at higher magnification (c, d) show new bone (B) in the pores of the oriented scaffolds (S) at 12 weeks and 24 weeks. Arrows indicate the edges of the old bone. Scale bar = 1 mm for (a,b and e–h), and 200 μm for (c, d).

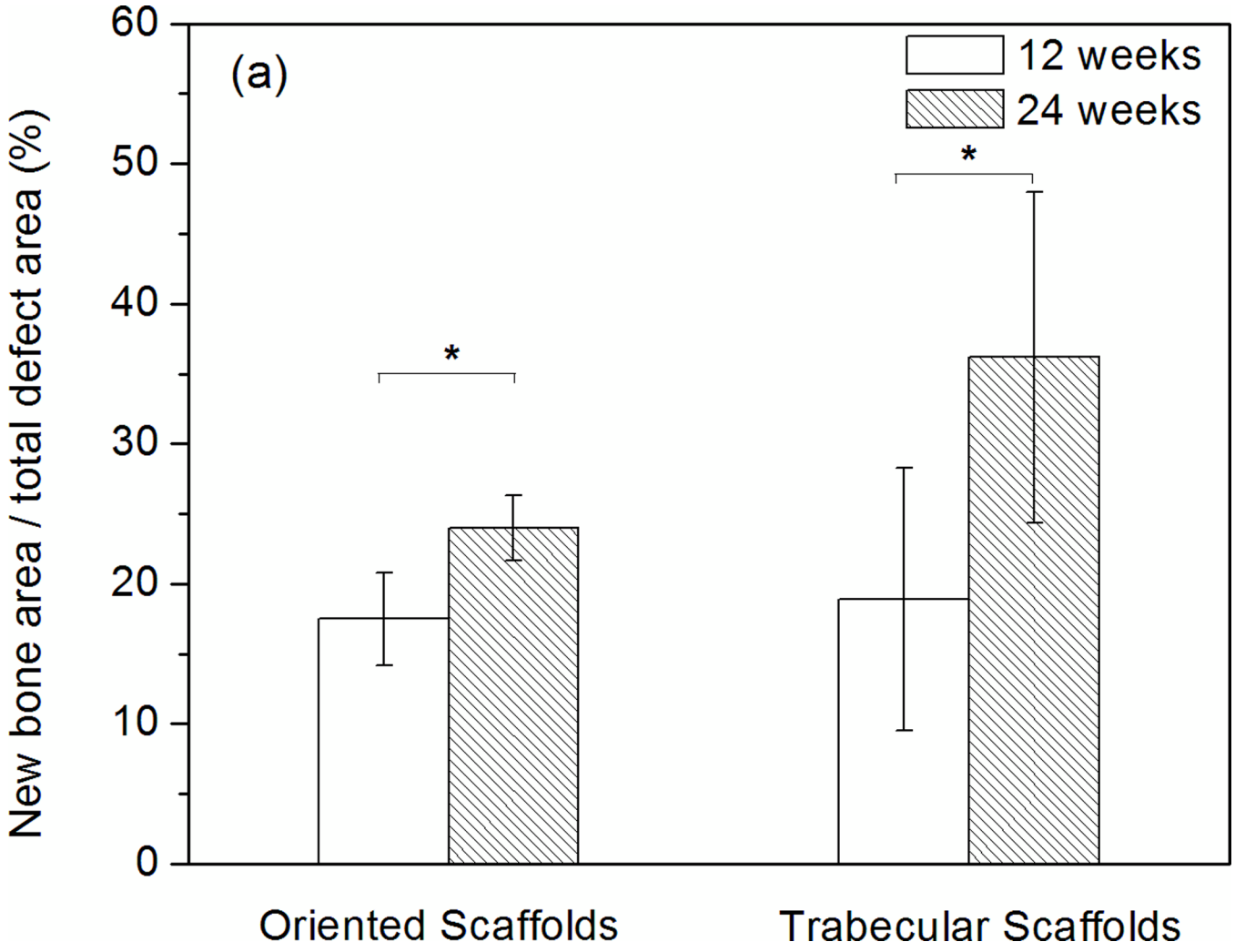

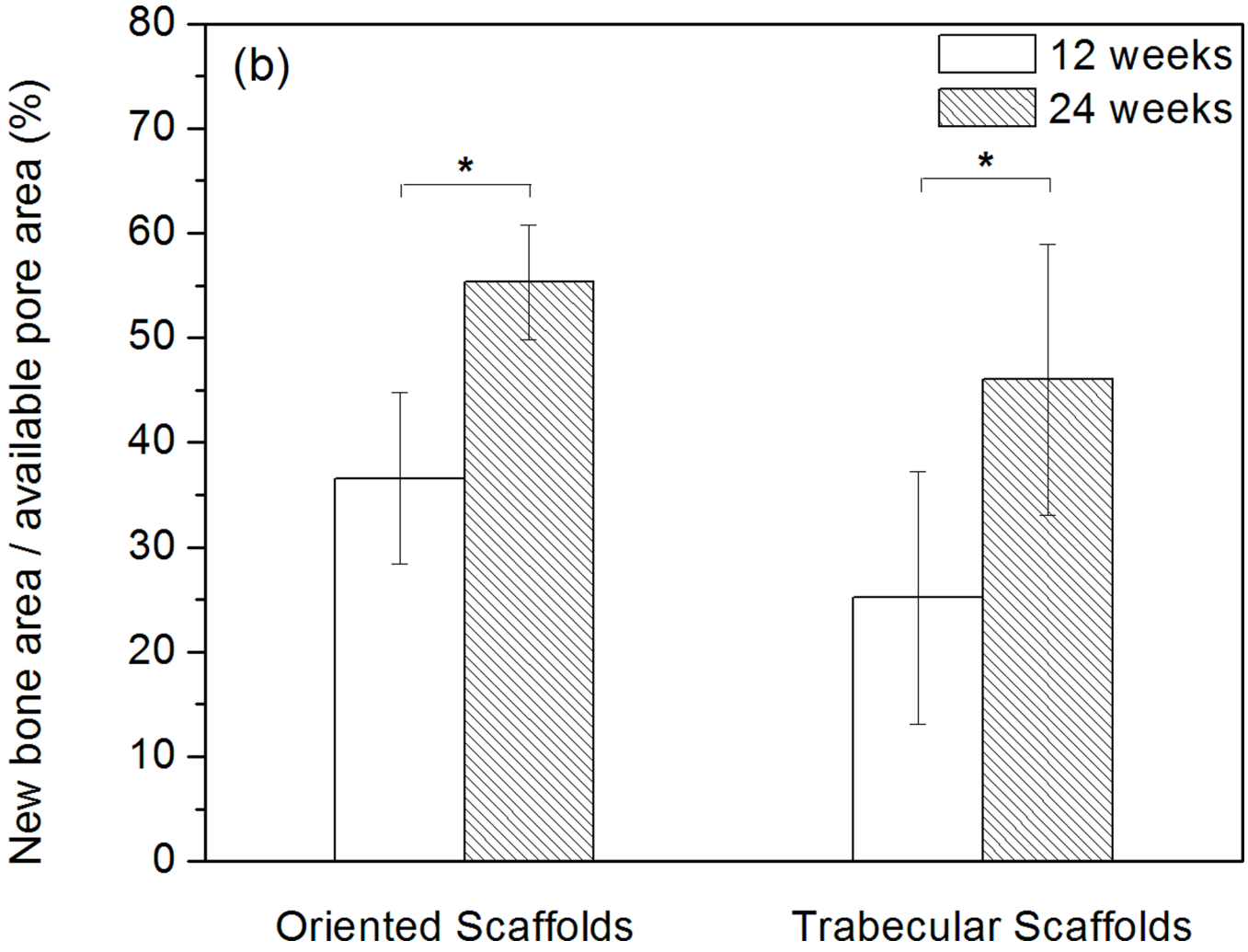

Fig. 4.

Histomophometric analysis of H&E stained sections showing total bone regeneration in rat calvarial defects implanted with oriented and trabecular scaffolds at 12 and 24 weeks: (a) normalized to the total defect area; (b) normalized to the available pore area of the scaffolds (*significant difference between scaffolds: $p<0.05$).

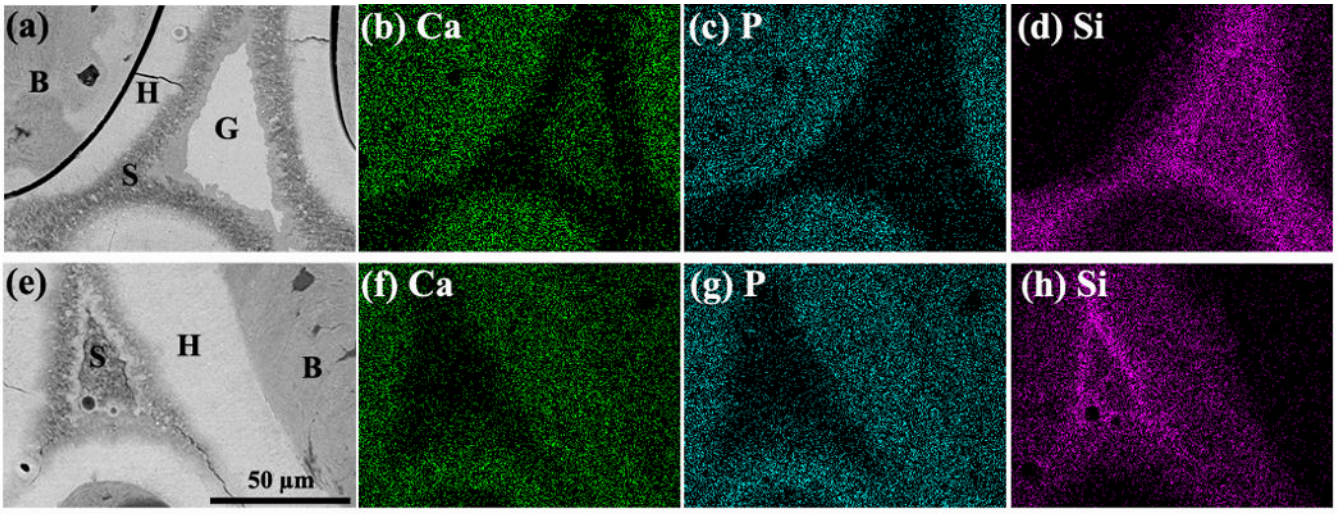

Fig. 5.

SEM backscattered electron images and X-ray maps for Ca (K), P(K) and Si(K) for oriented bioactive glass scaffolds after implantation for 12 weeks (a–d) and 24 weeks (e–h) in rat calvarial defects. Mineralized tissue (B) was formed adjacent to the hydroxyapatite (HA)-like layer (H) formed on the surface of the glass. G denotes the unconverted glass, and S the SiO_2-rich layer or SiO_2-rich core.

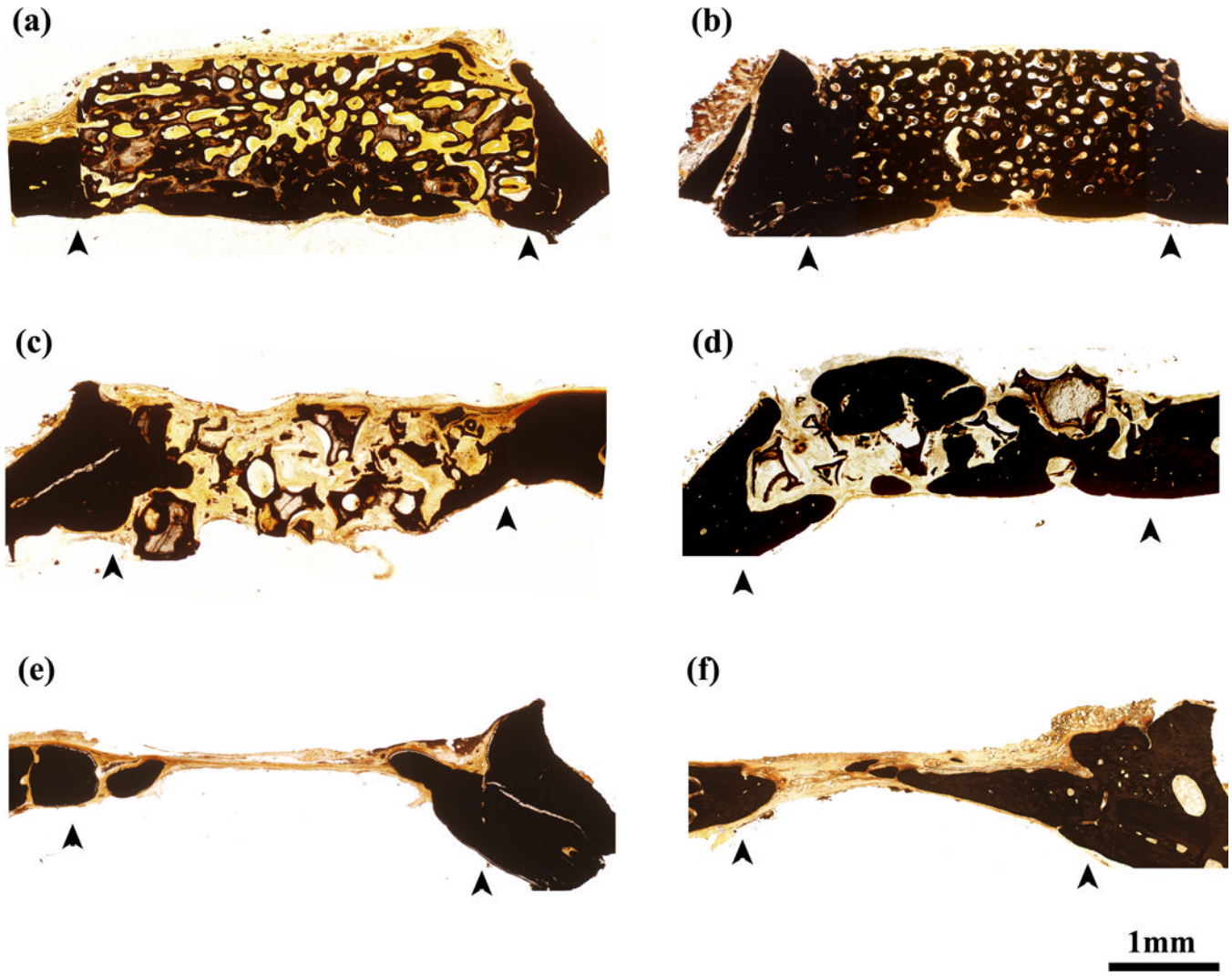

Fig. 6.
Von Kossa stained sections of rat calvarial defects implanted with oriented scaffolds at 12 weeks (a) and 24 weeks (b), defects implanted with trabecular scaffolds at 12 weeks (c) and 24 weeks (d), and empty defects at 12 weeks (e) and 24 weeks (f). Arrows indicate the edges of the old bone.

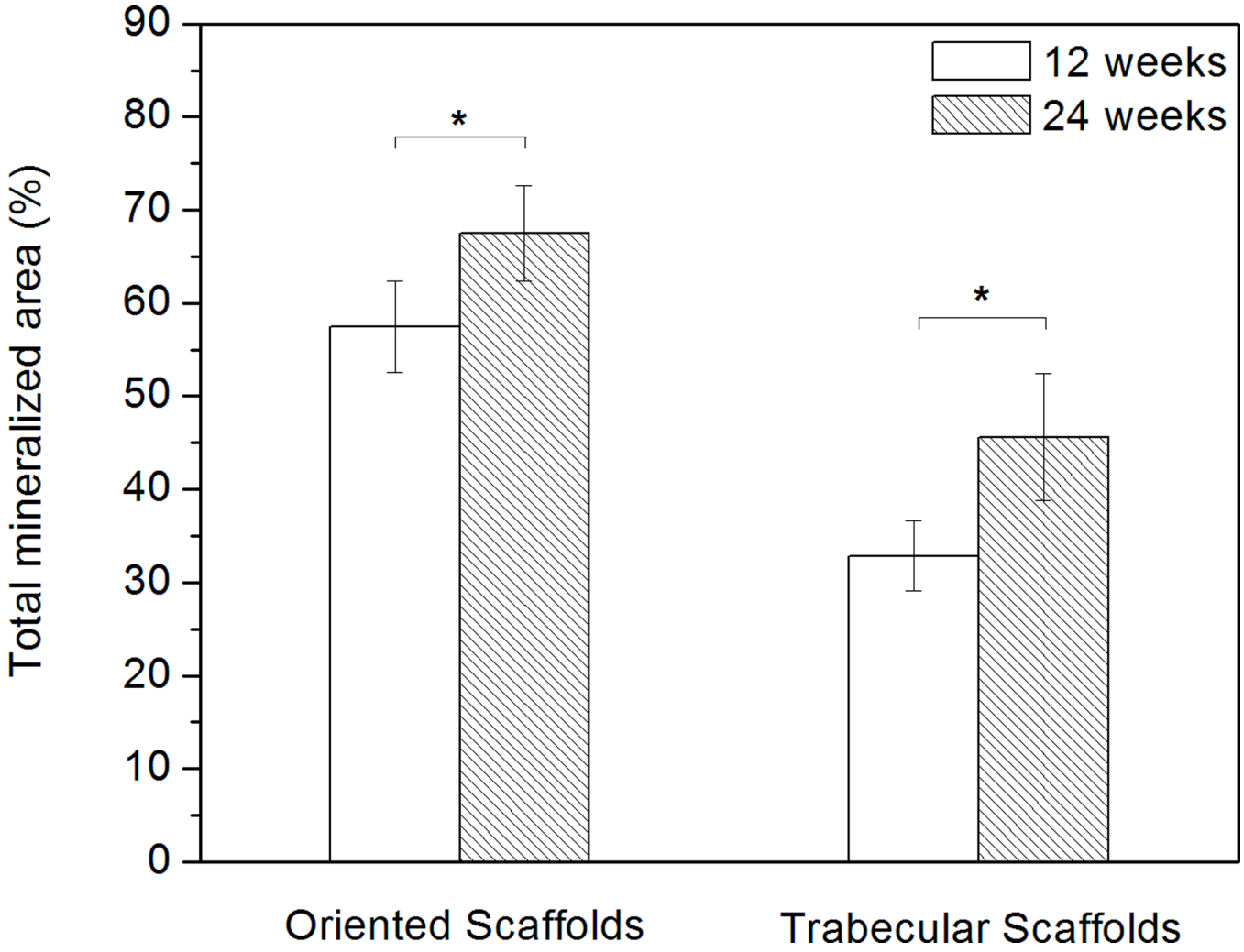

Fig. 7.
Histomophometric analysis of von Kossa positive area (total mineralized area of new bone and HA-like layer of scaffold) in rat calvarial defects implanted with oriented and trabecular scaffolds 12 weeks and 24 weeks postimplantation (*significant difference between scaffolds: $p<0.05$).

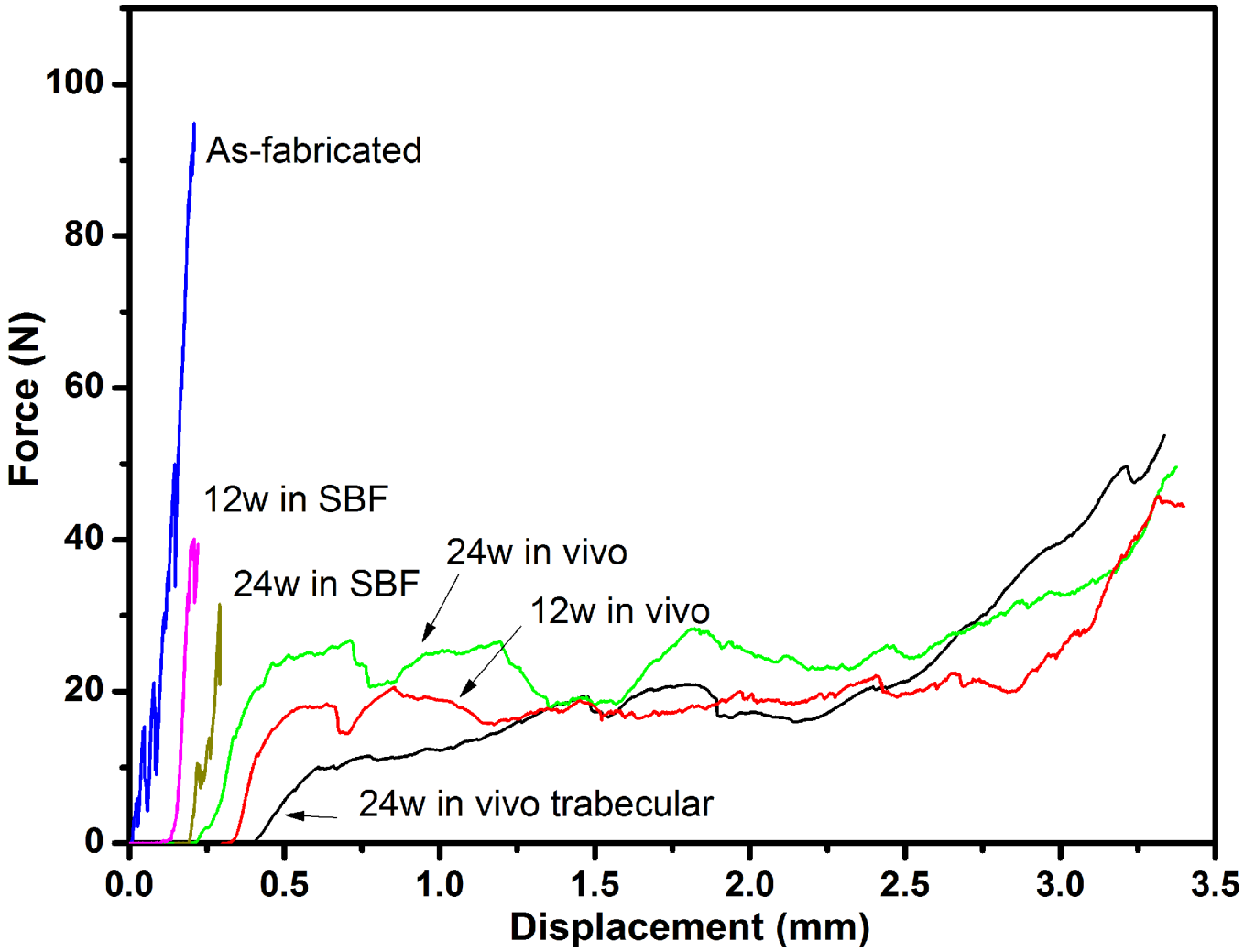

Fig. 8.

Force vs. displacement response for oriented scaffolds as fabricated, after immersion in SBF for 12 and 24 weeks, and after implantation in rat calvarial defects for 12 and 24 weeks. The response of trabecular scaffolds (positive control) after implantation for 24 weeks is also shown. (The curves were arbitrarily shifted along the *x*-axis to maintain clarity.)

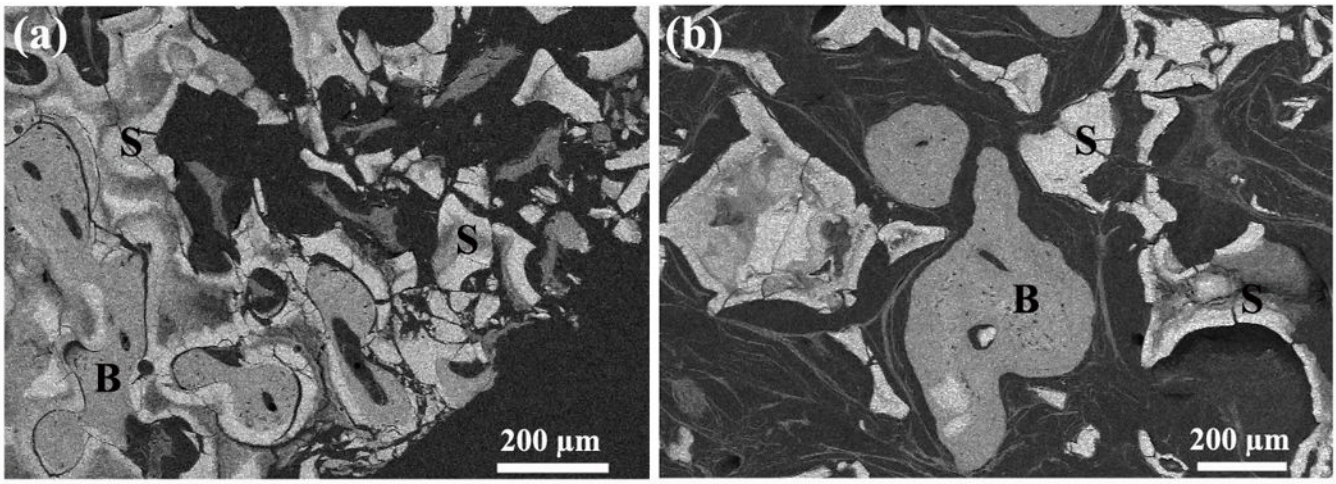

Fig. 9.
SEM backscattered images showing the cross-sections of (a) oriented scaffolds and (b) trabecular scaffolds after implantation in rat calvarial defects for 24 weeks and testing in the diametral compression test. (S: converted bioactive glass scaffold; B: mineralized tissue)

Table I

Characteristics of silicate 13–93 bioactive glass scaffolds with oriented and trabecular microstructure

Scaffold	Porosity (%)	Pore size (μm)	Compressive strength (MPa)	Elastic modulus (GPa)	Fabrication method
Oriented	50 ± 4	50–150	47 ± 5	11 ± 3	Unidirectional freezing of suspensions
Trabecular	80 ± 5	100–500	11 ± 1	3 ± 0.5	Polymer foam replication

Table II

EDS data for the Ca/P atomic ratio in different regions of 13–93 bioactive glass scaffold with an oriented microstructure after implantation for 12 and 24 weeks in rat calvarial defects. (The regions of the scaffold examined are shown in Fig. 5a, e).

Time (weeks)	Bone (B)	HA-like layer[1] (H)	SiO_2-rich layer/core (S)	Glass core (G)
12	1.72 ± 0.03	1.75 ± 0.04	2.6 ± 0.2	6.4 ± 0.4
24	1.52 ± 0.06	1.68 ± 0.03	1.9 ± 0.1	-

[1] Ca/P atomic ratio for stoichiometric HA = 1.67